In M. Pelillo, E. Hancock (Eds.):
Energy Minimization Methods in Computer Vision and Pattern Recognition.
Lecture Notes in Computer Science,
Vol. 10746, 409-423, Springer, Cham, 2018.
The final publication is available at link.springer.com.

Modelling Stable Backward Diffusion and Repulsive Swarms with Convex Energies and Range Constraints

Leif Bergerhoff[1], Marcelo Cárdenas[1], Joachim Weickert[1], and Martin Welk[2]

[1] Mathematical Image Analysis Group, Saarland University
Campus E1.7, 66041 Saarbrücken, Germany
{bergerhoff,cardenas,weickert}@mia.uni-saarland.de
[2] Institute of Biomedical Image Analysis
Private University for Health Sciences, Medical Informatics and Technology
Eduard-Wallnöfer-Zentrum 1, 6060 Hall/Tyrol, Austria
martin.welk@umit.at

Abstract. Backward diffusion and purely repulsive swarm dynamics are generally feared as ill-posed, highly unstable processes. On the other hand, it is well-known that minimising strictly convex energy functionals by gradient descent creates well-posed, stable evolutions. We prove a result that appears counterintuitive at first glance: We derive a class of one-dimensional backward evolutions from the minimisation of strictly convex energies. Moreover, we stabilise these inverse evolutions by imposing range constraints. This allows us to establish a comprehensive theory for the time-continuous evolution, and to prove a stability condition for an explicit time discretisation. Prototypical experiments confirm this stability and demonstrate that our model is useful for global contrast enhancement in digital greyscale images and for modelling purely repulsive swarm dynamics.

Keywords: Convex Optimisation, Inverse Processes, Dynamical Systems, Diffusion Filtering, Swarm Dynamics

1 Introduction

Backward parabolic partial differential equations such as inverse diffusion are classical representatives of ill-posed processes. For nonsmooth initial data, they may have no solution at all. Even if a solution exists, it is highly sensitive and

intrinsically unstable: Already the smallest perturbations of the initial data can cause huge deviations during the evolution.

Nevertheless, since forward parabolic equations can blur or smooth images, there have been a number of attempts to invert these evolutions for deblurring or sharpening degraded imagery. This, however, requires additional stabilisation. The most widely used strategy is to impose constraints at extrema that aim at enforcing a maximum–minimum principle. One example is the inverse diffusion filter of Osher and Rudin [4], which implements backward diffusion everywhere except at extrema, where the evolution is set to zero. Another example is the so-called forward-and-backward (FAB) diffusion of Gilboa et al. [3]. It differs from the closely related Perona–Malik filter [5] by the fact that it uses negative diffusivities for a specific range of gradient magnitudes. However, at extrema where the gradient vanishes, it always avoids explosions by imposing forward diffusion. So far any attempt to adequately implement inverse diffusions with forward or zero diffusion at extrema requires sophisticated numerical schemes [4, 8].

A second, less widely-used class of stabilisation attempts adds a fidelity term that prevents the backward evolution to move too far away from the original image [7] or from the average grey value of the desired range [6]. In this case the range of the filtered image obviously depends on the weights of the fidelity and the backward diffusion term.

In conclusion, we see that handling backward diffusion in practice is problematic and requires specific care to keep some sort of stability.

In order to gain new insights how to end up with stable backward evolutions, let us for a moment turn our attention to forward diffusion processes. For simplicity we consider a simple 1-D evolution for signal smoothing. It regards the original signal $f : [a, b] \to \mathbb{R}$ as initial state of the diffusion equation

$$\partial_t u = \partial_x \big(g(u_x^2)\, u_x \big) \tag{1}$$

where $u = u(x, t)$ is a filtered version of the original signal $u(x, 0) = f(x)$, $u_x = \partial_x u$, and reflecting boundary conditions at $x = a$ and $x = b$ are imposed. Larger diffusion times t create simpler representations. The diffusivity function g is nonnegative. In order to smooth less at signal edges than in more homogeneous regions, Perona and Malik [5] propose to choose g as a decreasing function of the contrast u_x^2. If the flux function $\Phi(u_x) := g(u_x^2)\, u_x$ is strictly increasing in u_x we have a forward diffusion process that cannot sharpen edges. Then the diffusion process can be seen as a gradient descent evolution for minimising the energy

$$E[u] = \int_a^b \Psi(u_x^2)\, dx \tag{2}$$

with a potential function $\tilde{\Psi}(u_x) = \Psi(u_x^2)$ that is strictly convex in u_x, increasing in u_x^2, and satisfies $\Psi'(u_x^2) = g(u_x^2)$. Since the energy functional is strictly convex, it has a unique minimiser. This minimiser is given by the (flat) steady state ($t \to \infty$) of the gradient descent method, and the gradient descent / diffusion

evolution is well-posed. Due to this classical appearance of well-posed forward diffusion as a consequence of strictly convex energies, one might be tempted to believe that backward diffusion is necessarily connected to nonconvex energies. Interestingly, this is not correct! Understanding this connection better opens new ways to design stable backward processes.

Our Contribution. We consider a space-discrete model where we admit *globally negative* diffusivities, corresponding to decreasing penalisers Ψ. However, we require $\Psi(u_x^2)$ to be strictly convex in u_x. We do not rely on stabilisations through zero or forward diffusivities at extrema, and we do not incorporate fidelity terms explicitly. Stabilisation will be achieved in our model on a *global* level by bounding the range of u. This is achieved by imposing reflecting boundary conditions in the co-domain. We show that this is sufficient to stabilise the inverse diffusion in the space-discrete and time-continuous setting. We also prove that a straightforward explicit time discretisation inherits this stability, if it satisfies a suitable time step size restriction. Our model opens up interesting applications in signal and image filtering, where it can be used for global contrast enhancement, as well as in swarm-like particle systems with purely repulsive interactions.

Structure of the Paper. In Section 2 we introduce our novel one-dimensional model and present a comprehensive analysis of its theoretical properties. The third section establishes stability bounds for an explicit time discretisation. Section 4 deals with the application of our model to image enhancement and the modelling of swarm behaviour. Finally, Section 5 gives conclusions and an outlook on future challenges.

2 Model and Theory

2.1 Discrete Variational Model

We start by introducing a dynamical system that is motivated from a spatial discretisation of the energy functional (2) with a decreasing penaliser function $\Psi : \mathbb{R}_0^+ \to \mathbb{R}$ and a global range constraint on u. The corresponding flux function Φ is given by $\Phi(s) := \Psi'(s^2)s$.

We consider vectors $\boldsymbol{v} = (v_1, \dots, v_N)^{\mathrm{T}} \in (0,1)^N$, where v_i for $i = 1, \dots, N$ are assumed to be distinct. We extend such $\boldsymbol{v}$ with the additional coordinates $v_{N+1}, \dots, v_{2N}$ defined as $v_{2N+1-i} = 2 - v_i \in (1,2)$. For this extended $\boldsymbol{v} \in [0,2]^{2N}$, we consider the energy function

$$E(\boldsymbol{v}) = \frac{1}{4} \cdot \sum_{i=1}^{2N} \sum_{j=1}^{2N} \Psi\big((v_j - v_i)^2\big) \ . \tag{3}$$

which models the repulsion potential between all positions v_i and v_j. A typical scenario for Ψ is illustrated in Figure 1. First, the function $\Psi(s^2)$ is defined as a continuously differentiable, decreasing, and strictly convex function for $s \in [0,1]$

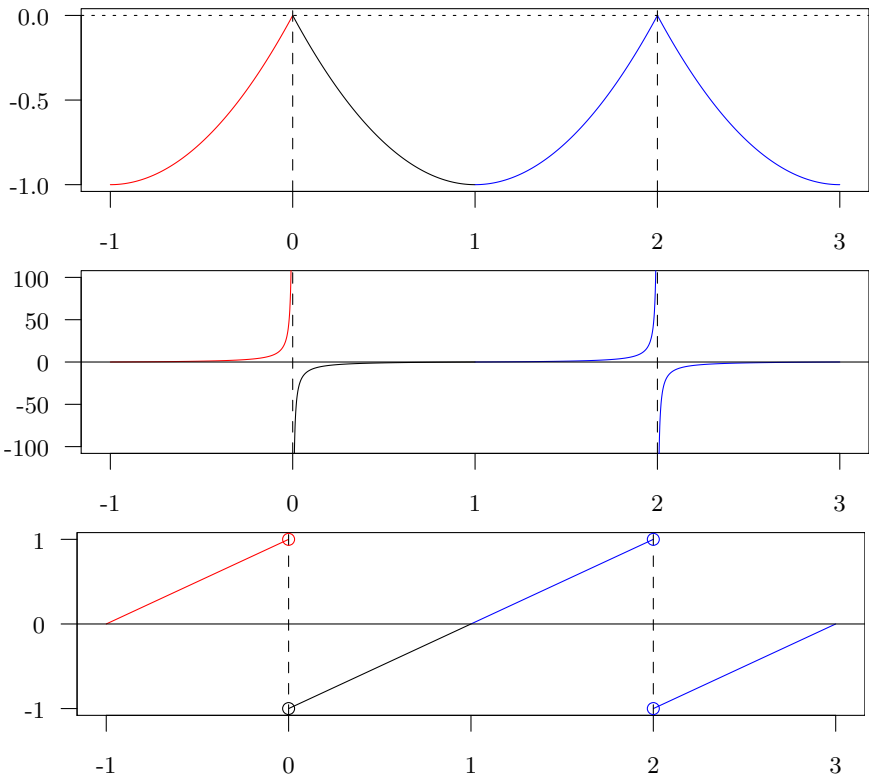

Fig. 1. Top: Exemplary penaliser $\tilde{\Psi}(s) := \Psi(s^2)$ with $\tilde{\Psi}(s) = (s-1)^2 - 1$ for $s \in [0,1]$, extended to the interval $[-1,3]$ by imposing symmetry and $\Psi((2+s)^2) = \Psi(s^2)$. **Middle:** Corresponding diffusivity $\tilde{g}(s) := g(s^2) = \Psi'(s^2)$ where $\tilde{g}(s) := 1 - 1/s$ for $s \in (0,1]$. **Bottom:** Corresponding flux $\Phi(s) = \Psi'(s^2)s$ with $\Phi(s) = s - 1$ for $s \in (0,1]$.

with $\Psi(0) = 0$ and $\Phi_-(1) = 0$ (left-sided derivative). It is then extended to $[-1,1]$ by symmetry and to $\mathbb{R}$ by periodicity $\Psi\big((2+s)^2\big) = \Psi(s^2)$. As a result, $\Psi(s^2)$ is continuously differentiable everywhere except at even integers, where it is still continuous. Note that $\Psi(s^2)$ is increasing on $[-1,0]$ and $[1,2]$. The flux Φ is continuous and increasing in $(0,2)$ with jump discontinuities at 0 and 2 (see Figure 1). Furthermore, we have that $\Phi(s) = -\Phi(-s)$ and $\Phi(2+s) = \Phi(s)$. A gradient descent for (3) is given by

$$\partial_t v_i = -\partial_{v_i} E(\boldsymbol{v}) = \sum_{\substack{j=1 \\ j \neq i}}^{2N} \Phi(v_j - v_i) \ , \quad i = 1, \dots, 2N \ , \tag{4}$$

where v_i now are functions of the time t. Note that for $1 \leq i, j \leq N$, thus $|v_j - v_i| < 1$, the flux $\Phi(v_j - v_i)$ is negative for $v_j > v_i$ and positive otherwise, thus driving v_i always away from v_j. This implies that we have negative diffusivities

Ψ' for all $|v_j - v_i| < 1$. Due to the convexity of $\Psi(s^2)$, the absolute values of the repulsive forces Φ are decreasing with the distance between v_i and v_j. We remark that the jumps of Φ at 0 and 2 are not problematic here as the v_i are required to be distinct.

Let us discuss shortly how the interval constraint for the v_i, $i = 1, \dots, N$, is enforced in (3) and (4). First, notice that v_{2N+1-i} for $i = 1, \dots, N$ is the reflection of v_i on the right interval boundary 1. For v_i and v_{2N+1-j} with $1 \leq i, j \leq N$ and $v_{2N+1-j} - v_i < 1$ there is a repulsive force due to $\Phi(v_{2N+1-j} - v_i) < 0$ that drives v_i and v_{2N+1-j} away from the *right* interval boundary. The closer v_i and v_{2N+1-j} come to this boundary, the stronger is the repulsion. For $v_{2N+1-j} - v_i > 1$, we have $\Phi(v_{2N+1-j} - v_i) > 0$. By $\Phi(v_{2N+1-j} - v_i) = \Phi\big((2 - v_j) - v_i\big) = \Phi\big((-v_j) - v_i\big)$, this can equally be interpreted as a repulsion between v_i and $-v_j$ where $-v_j$ is the reflection of v_j at the left interval boundary 0. In this case the interaction between v_i and v_{2N+1-j} drives v_i and $-v_j$ away from the *left* interval boundary. Recapitulating both possible cases, it becomes clear that every v_i is either repelled from the reflection of v_j at the left or at the right interval boundary, but never from both at the same time.

As $\partial_t v_{2N+1-i} = -\partial_t v_i$ holds in (4), the symmetry of $\boldsymbol{v}$ is preserved. Dropping the redundant entries $v_{N+1}, \dots, v_{2N}$, equation (4) can be rewritten as

$$\partial_t v_i = \sum_{\substack{j=1 \\ j \neq i}}^{N} \Phi(v_j - v_i) - \sum_{j=1}^{N} \Phi(v_i + v_j) \ , \quad i = 1, \dots, N \ , \tag{5}$$

where the second sum represents the repulsions between original and reflected coordinates in a more symmetric way.

Given an initial vector $\boldsymbol{f} \in (0,1)^N$ with distinct entries f_i, and initialising $v_i(0) = f_i$, $v_{2N+1-i}(0) = 2 - f_i$ for $i = 1, \dots, N$, the gradient descent (4) or (5) evolves $\boldsymbol{v}$ towards a minimiser of E.

A more detailed analysis below shows that in the course of the evolution, no v_i can reach the interval boundaries 0 or 1, and no v_i, v_j with $i \neq j$ can ever become equal. Thus the initial rank-order of v_i is preserved throughout the evolution. Each of the $N!$ possible rank-orders constitutes a connected component of the configuration space for $\boldsymbol{v}$. There is a unique minimiser of E in the interior of each connected component due to the strict convexity of $\Psi(s^2)$.

Theorem 1 (Avoidance of Boundaries). *The N initially distinct positions $v_i \in (0,1)$ evolving according to (5) never reach the domain boundaries 0 and 1.*

Proof. The definition of Ψ implies that

$$\lim_{h \to 0^+} \frac{\Psi\left((0+h)^2\right) - \Psi(0)}{h} < 0 \quad \text{and} \quad \lim_{h \to 0^-} \frac{\Psi(2^2) - \Psi\left((2+h)^2\right)}{h} > 0 \ , \tag{6}$$

from which it follows that

$$\lim_{v_i \to 0^+} \big(- \Phi(2v_i) \big) > 0 \quad \text{and} \quad \lim_{v_i \to 1^-} \big(- \Phi(2v_i) \big) < 0 \ . \tag{7}$$

Equation (5) can be written as

$$\partial_t v_i = \sum_{\substack{j=1 \\ j\neq i}}^{N} \big(\Phi(v_j - v_i) - \Phi(v_i + v_j)\big) - \Phi(2v_i) \ . \tag{8}$$

Since for $j = 1, \ldots, N$ and $j \neq i$ one has

$$\lim_{v_i \to 0^+} \Phi(v_j - v_i) - \Phi(v_i + v_j) = 0 \quad \text{and} \quad \lim_{v_i \to 1^-} \Phi(v_j - v_i) - \Phi(v_i + v_j) = 0 \ , \tag{9}$$

it follows that

$$\lim_{v_i \to 0^+} \partial_t v_i > 0 \quad \text{and} \quad \lim_{v_i \to 1^-} \partial_t v_i < 0 \ . \tag{10}$$

Consequently, v_i can never reach the left interval boundary 0 because it will move to the right when getting closer to it. The same holds for the right domain boundary 1 where v_i will move to the left before reaching it. □

Theorem 2 (Nonequality of v_i and v_j). *Among N initially distinct positions $v_i \in (0, 1)$ evolving according to (5), no two ever become equal.*

Proof. Using (5) it is possible to derive the difference

$$\begin{aligned} \partial_t \left(v_j - v_i\right) = 2 \cdot \Phi(v_i - v_j) + \sum_{\substack{k=1 \\ k\neq i,j}}^{N} \big(\Phi(v_k - v_j) - \Phi(v_k - v_i)\big) \\ - \sum_{k=1}^{N} \big(\Phi(v_j + v_k) - \Phi(v_i + v_k)\big) \end{aligned} \tag{11}$$

where $1 \leq i, j \leq N$. Assume w.l.o.g. that $v_j > v_i$ and consider (11) in the limit $v_j - v_i \to 0$. Then we have

$$\lim_{v_j - v_i \to 0} \partial_t (v_j - v_i) = \lim_{v_j - v_i \to 0} 2 \cdot \Phi(v_i - v_j) > 0 \ . \tag{12}$$

The latter inequality follows from the fact that $\Phi(s) > 0$ for $s \in (-1, 0)$. This means that v_j will always start moving away from v_i (and vice versa) when the difference between both gets sufficiently small. Since the initial positions are distinct, it follows that $v_i \neq v_j$ for $i \neq j$ for all times t. □

Theorem 3 (Explicit Steady-State Solution). *Under the assumption that (v_i) is in increasing order and that $\Psi(s^2)$ is twice continuously differentiable in $(0, 2)$ the unique minimiser of (3) is given by $\boldsymbol{v}^* = (v_1^*, \ldots, v_{2N}^*)^{\mathrm{T}}$, $v_i^* = (i - 1/2)/N$, $i = 1, \ldots, 2N$.*

Proof. Equation (3) can be rewritten without the redundant entries of $\boldsymbol{v}$ as

$$E(\boldsymbol{v}) = 2 \cdot \sum_{i=1}^{N-1} \sum_{j=i+1}^{N} \Psi\big((v_j - v_i)^2\big) + \sum_{i=1}^{N} \Psi(4v_i^2) + 2 \cdot \sum_{i=1}^{N-1} \sum_{j=i+1}^{N} \Psi\big((v_i + v_j)^2\big) \tag{13}$$

from which one can verify by straightforward, albeit lengthy calculations that $\boldsymbol{\nabla} E(\boldsymbol{v}^*) = 0$, and the Hessian of E at $\boldsymbol{v}^*$ is

$$\mathrm{D}^2 E(\boldsymbol{v}^*) = \sum_{k=1}^{N} \boldsymbol{A}_k \Phi'\left(\frac{k}{N}\right) \tag{14}$$

with sparse symmetric $N \times N$-matrices

$$\boldsymbol{A}_k = 4\boldsymbol{I} - 2\boldsymbol{T}_k - 2\boldsymbol{T}_{-k} + 2\boldsymbol{H}_{k+1} + 2\boldsymbol{H}_{2N-k+1} \ , \quad k = 1, \ldots, N-1 \ , \tag{15}$$

$$\boldsymbol{A}_N = 2\boldsymbol{I} + 2\boldsymbol{H}_{N+1} \tag{16}$$

where the unit matrix $\boldsymbol{I}$, single-diagonal Toeplitz matrices $\boldsymbol{T}_k$ and single-anti-diagonal Hankel matrices $\boldsymbol{H}_k$ are defined as

$$\boldsymbol{I} = \left(\delta_{i,j}\right)_{i,j=1}^{N} \ , \qquad \boldsymbol{T}_k = \left(\delta_{j-i,k}\right)_{i,j=1}^{N} \ , \qquad \boldsymbol{H}_k = \left(\delta_{i+j,k}\right)_{i,j=1}^{N} \ . \tag{17}$$

Here, $\delta_{i,j}$ denotes the Kronecker symbol, $\delta_{i,j} = 1$ if $i = j$, and $\delta_{i,j} = 0$ otherwise. All $\boldsymbol{A}_k$, $k = 1, \ldots, N$ are weakly diagonally dominant with positive diagonal, thus positive semidefinite by Gershgorin's Theorem. Moreover, the tridiagonal matrix $\boldsymbol{A}_1$ is of full rank, thus even positive definite. By strict convexity of $\Psi(s^2)$, all $\Phi'(k/N)$ are positive, thus $\mathrm{D}^2 E(\boldsymbol{v}^*)$ is positive definite.

As a consequence, the steady state of the gradient descent (5) for any initial data $\boldsymbol{f}$ (with arbitrary rank-order) can be computed directly by sorting the f_i: Let σ be the permutation of $\{1, \ldots, N\}$ for which $(f_{\sigma^{-1}(i)})_{i=1,\ldots,N}$ is increasing (this is what a sorting algorithm computes), the steady state is given by $v_i^* = (\sigma(i) - 1/2)/N$ for $i = 1, \ldots, N$. □

Theorem 4 (Convergence). *For $t \to \infty$ any initial configuration $\boldsymbol{v} \in (0,1)^N$ with distinct entries converges to a unique steady state $\boldsymbol{v}^*$ which is the global minimiser of the energy given in* (13).

Proof. As a sum of convex functions, (13) is convex. Therefore the function $V(\boldsymbol{v}) := E(\boldsymbol{v}) - E(\boldsymbol{v}^*)$ (where $\boldsymbol{v}^*$ is the equilibrium point) is a Lyapunov function with $V(\boldsymbol{v}^*) = 0$ and $V(\boldsymbol{v}) > 0$ for all $\boldsymbol{v} \neq \boldsymbol{v}^*$. Furthermore, we have

$$\partial_t V(\boldsymbol{v}) = -\sum_{i=1}^{N} \left(\partial_{v_i} E(\boldsymbol{v})\right)^2 \leq 0 \ . \tag{18}$$

Note that due to the positive definiteness of (14) we know that $E(\boldsymbol{v})$ has a strict (global) minimum which implies that the inequality in (18) becomes strict except in case of $\boldsymbol{v} = \boldsymbol{v}^*$. This guarantees asymptotic Lyapunov stability of $\boldsymbol{v}^*$ and thus convergence to $\boldsymbol{v}^*$ for $t \to \infty$. □

2.2 Generalisation with Weights

Let us now consider a generalised version of our model that allows for localisation and different treatment of distinct v_i. For this purpose we make use of vectors

$\boldsymbol{w} = (w_1, \dots, w_N)^{\mathrm{T}} \in (0, \infty)^N$ and $\boldsymbol{x} = (\boldsymbol{x}_1, \dots, \boldsymbol{x}_N)^{\mathrm{T}} \in (\mathbb{R}^n)^N$ which we extend – similar to $\boldsymbol{v}$ – with the coordinates $w_{N+1}, \dots, w_{2N}$ and $\boldsymbol{x}_{N+1}, \dots, \boldsymbol{x}_{2N}$. Both are defined as $w_{2N+1-i} = w_i$ and $\boldsymbol{x}_{2N+1-i} = \boldsymbol{x}_i$. Each w_i denotes the weight, or importance, of the corresponding v_i, whereas the $\boldsymbol{x}_i$ provide additional n-dimensional position information which will become relevant in our future research. Neither w_i nor $\boldsymbol{x}_i$ change over time. Additionally, we introduce a weighting function $\gamma\big(|x|\big)$ which is 1 for $|x| \leq \varrho$ and 0 else for $\varrho > 0$. Now regard the adapted variant of (3) given by

$$E(\boldsymbol{p}, \boldsymbol{x}, \boldsymbol{w}) = \frac{1}{4} \sum_{i=1}^{2N} \sum_{j=1}^{2N} w_i \cdot w_j \cdot \gamma\big(|\boldsymbol{x}_j - \boldsymbol{x}_i|\big) \cdot \Psi \left(\left(\frac{p_j}{\sqrt{w_j}} - \frac{p_i}{\sqrt{w_i}} \right)^2 \right), \quad (19)$$

where we make use of the coordinate transform $p_i := \sqrt{w_i} \cdot v_i$, $i = 1, \dots, 2N$. Referring to (4), a gradient descent can be formulated as

$$\partial_t p_i = \sqrt{w_i} \cdot \sum_{\substack{j=1 \\ j \neq i}}^{2N} w_j \cdot \gamma\big(|\boldsymbol{x}_j - \boldsymbol{x}_i|\big) \cdot \Phi \left(\frac{p_j}{\sqrt{w_j}} - \frac{p_i}{\sqrt{w_i}} \right) \quad (20)$$

for $i = 1, \dots, 2N$. Since $\partial_t p_{2N+1-i} = -\partial_t p_i$, we can drop the redundant entries and rewrite (20) with $\partial_t p_i = \sqrt{w_i} \cdot \partial_t v_i$ for $i = 1, \dots, N$ as

$$\partial_t v_i = \sum_{\substack{j=1 \\ j \neq i}}^{N} w_j \cdot \gamma\big(|\boldsymbol{x}_j - \boldsymbol{x}_i|\big) \cdot \Phi(v_j - v_i) - \sum_{j=1}^{N} w_j \cdot \gamma\big(|\boldsymbol{x}_j - \boldsymbol{x}_i|\big) \cdot \Phi(v_i + v_j) \ . \quad (21)$$

Properties of the Generalised Model. Proceeding similar as in Section 2.1 it can be shown that Theorem 1 also holds for the generalised model. Theorem 2 applies for all pairs v_i, v_j with $|\boldsymbol{x}_i - \boldsymbol{x}_j| \leq \varrho$. A minimiser $\boldsymbol{p}^*$ for $E(\boldsymbol{p}, \boldsymbol{x}, \boldsymbol{w})$ depends in general on the definition of Ψ. As evident from Theorem 3 this dependency vanishes in the special case $\gamma = 1$, $w_i = 1$, for $i = 1, \dots, N$. For nontrivial w_i we assume for the moment that Φ belongs to the class of linear functions, i.e. $\Phi(s) = a \cdot (s - 1)$, $a > 0$ (cf. Figure 1). For adequate ϱ – implying $\gamma = 1$ for all pairs $(\boldsymbol{x}_i, \boldsymbol{x}_j)$ – our model acts globally and we get

$$p_i^* = \sqrt{w_i} \cdot v_i^* = \sqrt{w_i} \cdot \frac{\sum_{j=1}^{i} w_j - \frac{1}{2} w_i}{\sum_{j=1}^{N} w_j} \quad , \quad i = 1, \dots, N \quad (22)$$

as a sufficient condition for the elements of a global minimiser $\boldsymbol{p}^*$ (and $\boldsymbol{v}^*$). A restriction to linear functions Φ also allows to prove convergence in accordance with Theorem 4.

2.3 Relation to Variational Signal and Image Filtering

We will interpret $v_1, \dots, v_N$ as samples of a smooth 1D signal $u : \Omega \to [0,1]$ over an interval Ω of the real axis, taken at sampling positions $x_i = x_0 + i\,h$ with grid mesh size $h > 0$. We consider the model (19) with all w_i fixed to 1.

Theorem 5 (Space-Continuous Energy). *Equation* (19) *with* $w_i = 1$ *for all* i *can be considered as a discretisation of*

$$E[u] = \frac{1}{2} \int_\Omega \big(W(u_x^2) + B(u)\big)\,\mathrm{d}x \tag{23}$$

with penaliser $W(u_x^2) \approx C\,\Psi(u_x^2)$ *and barrier function* $B(u) \approx D\,\Psi(4u^2)$*, where* C *and* D *are positive constants.*

Remark 1. The function W represents a decreasing penaliser convex in u_x, whereas B denotes a convex barrier function that enforces the interval constraint on u by favouring values u away from the interval boundaries. The discrete penaliser Ψ generates both the penaliser W for derivatives and the barrier function B.

Remark 2. Note that by construction of W the diffusivity $g(u_x^2) := W'(u_x^2) \sim \Psi'(u_x^2)$ has a singularity at 0 with $-\infty$ as limit.

Remark 3. The cut-off of γ at radius ϱ implies the locality of the functional (23) that can thereby be linked to a diffusion equation of type (1). Without a cut-off, a nonlocal diffusion equation would arise instead.

Proof (of Theorem 5). We notice first that $v_j - v_i$ and $v_i + v_j$ for $1 \le i, j \le N$ are first-order approximations of $(j-i)\,h\,u_x(x_i)$ and $2u(x_i)$, respectively.

Derivation of the Penaliser W. Assume first for simplicity that $\Psi(s^2) = -\kappa s$, $\kappa > 0$ is linear in s on $[0,1]$ (thus not strictly convex). Then we have for a part of the inner sums of (19) corresponding to a fixed i

$$\begin{aligned}
&\frac{1}{2}\Big(\sum_{j=1}^{N} \gamma\big(|x_j - x_i|\big)\Psi\big((v_j - v_i)^2\big) + \sum_{j=N+1}^{2N} \gamma\big(|x_j - x_{2N+1-i}|\big)\Psi\big((v_j - v_{2N+1-i})^2\big)\Big) \\
&\quad = \sum_{j=1}^{N} \gamma\big(|x_j - x_i|\big) \cdot \Psi\big((|v_j - v_i|)^2\big) \approx -\kappa\,h\,u_x(x_i) \sum_{j=1}^{N} \gamma\big(|j-i|\,h\big) \cdot |j-i| \\
&\quad = h\,\Psi\big(u_x(x_i)^2\big) \sum_{k=1-i}^{N-i} |k|\,\gamma\big(|k|\,h\big) \approx h\,\Psi\big(u_x(x_i)^2\big)\lfloor\varrho\rfloor\big(\lfloor\varrho\rfloor + 1\big)
\end{aligned} \tag{24}$$

where in the last step the sum over $k = 1-i, \dots, N-i$ has been replaced with a sum over $k = -\lfloor\varrho\rfloor, \dots, \lfloor\varrho\rfloor$, thus introducing a cutoff error for those locations x_i that are within the distance ϱ from the interval ends. Summation over $i = 1, \dots, N$ approximates $\int_\Omega \lfloor\varrho\rfloor\big(\lfloor\varrho\rfloor + 1\big)\,\Psi(u_x^2)\,\mathrm{d}x$ from which we can read off $W(u_x^2) \approx \lfloor\varrho\rfloor\big(\lfloor\varrho\rfloor + 1\big)\Psi(u_x^2)$.

For $\Psi(s^2)$ that are non-linear in s, $\Psi(u_x(x_i)^2)$ in (24) is changed into a weighted sum of $\Psi\big((ku_x(x_i))^2\big)$ for $k = 1, \dots, N-1$, which still amounts to a decreasing function $W(u_x^2)$ that is convex in u_x. Qualitatively, W' then behaves the same way as before.

Derivation of the Barrier Function B. Collecting the summands of (19) that were not used in (24), we have, again for fixed i,

$$\frac{1}{2}\Big(\sum_{j=N+1}^{2N}\gamma\big(|x_j - x_i|\big)\Psi\big((v_j - v_i)^2\big) + \sum_{j=1}^{N}\gamma\big(|x_j - x_{2N+1-i}|\big)\Psi\big((v_j - v_{2N+1-i})^2\big)\Big)$$
$$= \sum_{j=1}^{N}\gamma\big(|x_j - x_i|\big)\Psi\big((v_i + v_j)^2\big) \approx \big(2\lfloor\varrho\rfloor + 1\big)\,\Psi\big(4u(x_i)^2\big)\ , \tag{25}$$

and thus after summation over i analogous to the previous step $\int_\Omega B(u)\,\mathrm{d}x$ with $B(u) \approx h^{-1}\big(2\lfloor\varrho\rfloor + 1\big)\,\Psi(4u^2)$. □

Similar derivations can be made for patches of $2D$ images. A point worth noticing is that the barrier function B is bounded. This differs from usual continuous models where such barrier functions tend to infinity at the interval boundaries. However, for each given sampling grid and patch size the barrier function is just strong enough to prevent W from pushing the values out of the interval.

3 Explicit Time Discretisation

Using forward differences to approximate the time derivative in (21) and using $\gamma_{i\ell} := \gamma\big(|\boldsymbol{x}_\ell - \boldsymbol{x}_i|\big)$ the explicit scheme of the generalised model reads

$$v_i^{k+1} = v_i^k + \tau\cdot\sum_{\substack{\ell=1\\ \ell\neq i}}^{N} w_\ell\cdot\gamma_{i\ell}\cdot\Phi(v_\ell^k - v_i^k) - \tau\cdot\sum_{\ell=1}^{N} w_\ell\cdot\gamma_{i\ell}\cdot\Phi(v_i^k + v_\ell^k),\quad i = 1, \dots, N, \tag{26}$$

where τ denotes the time step size and an upper index k refers to the time $k\tau$.

Theorem 6 (Stability Guarantees for the Explicit Scheme). *Let L_Φ be the Lipschitz constant of Φ restricted to the interval $(0, 2)$. Moreover, assume that the time step size used in the explicit scheme (26) satisfies $\tau < \left(2L_\Phi \sum_{i=1}^{N} w_i\right)^{-1}$. Then the following stability properties hold:*

(i) If $0 < v_i^k < 1$, then $0 < v_i^{k+1} < 1$, for every $1 \le i \le N$.
(ii) If $\gamma = 1$ and $0 < v_i^k < v_j^k < 1$, then $v_i^{k+1} < v_j^{k+1}$.

Proof. (i). Let $0 < v_i^k, v_j^k < 1$. We have the following three cases:
If $v_i^k < v_j^k$ then $v_j^k - v_i^k, v_i^k + v_j^k \in (0, 2)$. Thus,

$$\big|\Phi(v_i^k + v_j^k) - \Phi(v_j^k - v_i^k)\big| < L_\Phi \cdot 2v_i\ . \tag{27}$$

If $v_j^k < v_i^k \leq \frac{1}{2}$, then $v_j^k - v_i^k \in (-1, 0)$ and $v_j^k + v_i^k \in (0, 1)$. Thus,

$$0 \leq \Phi(v_j^k - v_i^k) - \Phi(v_i^k + v_j^k) \qquad \text{and} \qquad 0 \leq -\Phi(2v_i) \ . \tag{28}$$

Finally, if $v_j^k < v_i^k$ and $\frac{1}{2} < v_i^k$, using $\Phi(1) = 0$ and the periodicity of Φ we get

$$\begin{aligned} \left|\Phi(v_j^k - v_i^k) - \Phi(v_i^k + v_j^k)\right| = \left|\Phi(v_i^k + v_j^k) - \Phi(2 + v_j^k - v_i^k)\right| < 2v_i L_\Phi \qquad \text{and} \\ |\Phi(2v_i)| = |\Phi(2v_i) - \Phi(1)| \leq |2v_i - 1|\, L_\Phi \leq 2v_i L_\Phi \ . \end{aligned} \tag{29}$$

Combining (27), (28) and (29), we obtain that

$$\begin{aligned} &- \tau \cdot \sum_{\substack{\ell=1 \\ \ell \neq i}}^{N} w_\ell \cdot \gamma_{i\ell} \cdot \left(\Phi(v_i^k + v_\ell^k) - \Phi(v_\ell^k - v_i^k)\right) - \tau \cdot w_i \cdot \Phi(2v_i^k) \\ &< \ \tau \cdot L_\Phi \cdot 2v_i^k \cdot \sum_{\ell=1}^{N} w_\ell \ \ < \ \ v_i^k \ . \end{aligned} \tag{30}$$

This, together with (26) shows that $v_i^{k+1} > 0$, as claimed.
The proof of $v_i^{k+1} < 1$ proceeds in a similar way.

(ii). Considering the explicit discretisation of (26) for $\partial_t v_i$ and $\partial_t v_j$ and $\gamma = 1$, we obtain for $i, j = 1, \ldots, N$

$$\begin{aligned} v_j^{k+1} - v_i^{k+1} = \ & v_j^k - v_i^k + \tau \cdot (w_i + w_j) \cdot \Phi(v_i^k - v_j^k) + \\ & \tau \cdot \sum_{\substack{\ell=1 \\ \ell \neq i,j}}^{N} w_\ell \cdot \left(\Phi(v_\ell^k - v_j^k) - \Phi(v_\ell^k - v_i^k)\right) - \\ & \tau \cdot \sum_{\ell=1}^{N} w_\ell \cdot \left(\Phi(v_\ell^k + v_j^k) - \Phi(v_\ell^k + v_i^k)\right) \ . \end{aligned} \tag{31}$$

Using the fact that Φ is Lipschitz in the interval $(0, 2)$, we also know that

$$\begin{aligned} &\tau \cdot \sum_{\substack{\ell=1 \\ \ell \neq i,j}}^{N} w_\ell \cdot \left|\Phi(v_\ell^k - v_j^k) - \Phi(v_\ell^k - v_i^k)\right| + \tau \cdot \sum_{\ell=1}^{N} w_\ell \cdot \left|\Phi(v_\ell^k + v_j^k) - \Phi(v_\ell^k + v_i^k)\right| \\ &< \ \tau \cdot L_\Phi \cdot 2\,|v_j^k - v_i^k| \cdot \sum_{\ell=1}^{N} w_\ell \ \ < \ \ v_j^k - v_i^k \ . \end{aligned} \tag{32}$$

Finally, since $0 < \Phi(v_i^k - v_j^k)$, (31) and (32) imply that $0 < v_j^{k+1} - v_i^{k+1}$, as claimed. □

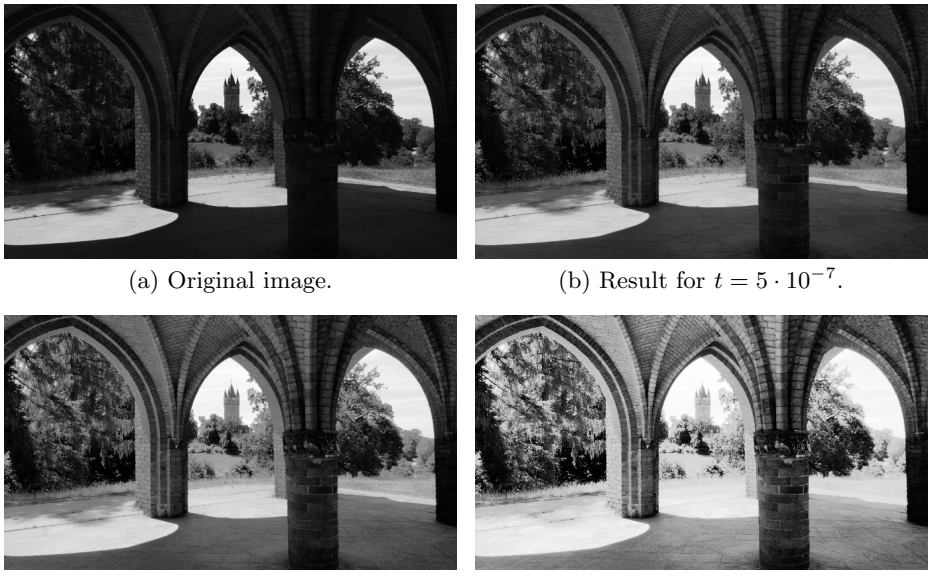

(a) Original image. (b) Result for $t = 5 \cdot 10^{-7}$.

(c) Result for $t = 10^{-6}$. (d) Steady state following (22).

Fig. 2. Processing a photography of "Flatowturm (Potsdam)" taken by the authors.

4 Applications

Image Enhancement. Similar to the approach proposed in [1] we apply our model to enhance the *global* contrast of digital grey value images $f : \{1, \dots, n_x\} \times \{1, \dots, n_y\} \to [0, 1]$. As illustrated in Figure 2, this can be achieved in two ways. The first option uses the explicit scheme (26) to describe the evolution of grey values v_i up to some time t (see Figure 2 (b) and (c)) where the weights w_i reflect the multiplicity of each grey value v_i. Note that all grey values are mapped to the interval $(0, 1)$ beforehand to ensure the validity of our model and γ is fixed to 1. The amount of contrast enhancement grows with increasing values of t. In our experiments an image size of 683×384 pixels and the application of a flux function Φ with $L_\Phi = 1$ (see Figure 1) imply an upper bound of $1/(2 \cdot 683 \cdot 384)$ for τ and allow us to achieve the presented results after just one iteration.

If one is only interested in an enhanced version of the original image with maximum global contrast there is an alternative, namely the derived steady state solution for linear flux functions (22). The result is shown in Figure 2 (d). Figure 2 also confirms that the solution of the explicit scheme (26) converges to the steady state solution (22) for $t \to \infty$. From (22) it is clear that the steady state is equivalent to histogram equalisation. It is therefore interesting to compare our evolution with the histogram modification flow introduced in [6] which can have the same steady state. Indeed, the flow from [6] can also be translated into a combination of repulsion among grey-values and a barrier function. However, as in [6] the repulsive force is constant, and the barrier function quadratic, they

cannot be derived from the same kind of interaction between the v_i and their reflected counterparts.

Repulsive Swarm Dynamics. Recent swarm models with individual particles often employ a pairwise potential $U : \mathbb{R}^n \to \mathbb{R}$ to model the attraction and repulsion behaviour among swarm mates (see e.g. [2] and the references therein). Physically simplified models describe the particle velocity directly (first order models):

$$\partial_t v_i = -\sum_{\substack{j=1 \\ j\neq i}}^{N} \nabla U\big(|v_i - v_j|\big) \ , \quad i = 1, \dots, N \ . \tag{33}$$

These models are often inspired by biology and describe long-term attractive and short-term repulsive behaviour between particles. The interplay of attractive and repulsive forces leads to flocking and allows to gain stability for the swarm. In the following we show that our model can be understood in terms of a purely repulsive first order swarm model. To the best of our knowledge there exists no model so far which restricts itself to pure repulsion among particles.

Our Purely Repulsive Swarm Model. Let $\boldsymbol{v} \in (0,2)^{2N}$ denote the extended vector of particle positions and $\boldsymbol{w} \in (0,\infty)^{2N}$ a constant vector containing the corresponding particle weights (extension of both vectors as described in Section 2.1 and Section 2.2). Then the evolution of particles is given by

$$\partial_t v_i = \sum_{\substack{j=1 \\ j\neq i}}^{2N} w_j \cdot \Phi(v_j - v_i) = \sum_{\substack{j=1 \\ j\neq i}}^{2N} w_j \cdot k(v_j - v_i) \cdot (v_j - v_i) \ , \quad i = 1, \dots, 2N \ , \tag{34}$$

where $k(s) = {}^{\Phi(s)}/_{s}$ for $s \neq 0$. The latter kernel function k describes the amount of repulsion between two particles and can also be interpreted in terms of a diffusivity $\Psi'(s^2)$. Comparing (33) and (34) it becomes clear that our model represents a first order swarm model which defines purely repulsive forces among N particles and their N reflections at the domain boundaries. A specific characteristic of our model compared to others is that it describes the repulsive movement of N particles in a closed system.

Results. Our experiments on purely repulsive swarm behaviour presented in Figure 3 and 4 illustrate the basic properties of our model. We start with a random initial particle distribution for $N = 7$ assuming that $v_i \in (0,1)$. In our first experiment (Figure 3) the initial weights w_i are set to 1 which results – as described in Section 2.1 – in a uniform distribution of the particles in the steady state. In the second experiment (Figure 4) we assume that the initial weights are given by $w_i = {}^1/_i$, for $i = 1, \dots, N$. These weights are illustrated by the area of the particles in Figure 4. We apply the linear flux function Φ from Figure 1. We notice that in the steady state given by (22), all particles are still in the same order as before. However, the distance between neighbouring particles varies and depends on the particle weights: the larger the weight, the larger the distance.

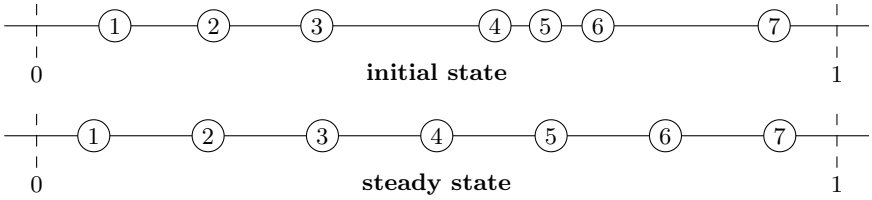

Fig. 3. Application of the model to a system of 7 particles with weights $w_i = 1$.

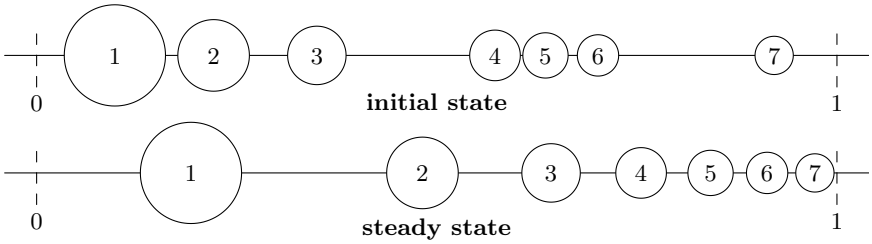

Fig. 4. Application of the model to a system of 7 particles with weights $w_i = 1/i$.

5 Summary and Conclusions

In our paper we have shown an unexpected result: Pure backward diffusion and fully repulsive swarm behaviour can be modelled as gradient descent of strictly convex energies. Moreover, we have demonstrated that it is neither necessary to impose forward or zero diffusion at extrema nor to add classical fidelity terms: Stability can already be guaranteed by reflecting boundary conditions in the diffusion co-domain or the domain of the positions of the swarm members. This stability carries over directly to a straightforward explicit scheme. No sophisticated numerics is required. A multi-dimensional extension of our model was left out for reasons of clarity and simplicity and is part of our current research.

We expect that our two key ingredients – convex energies combined with range constraints – are not only beneficial for modelling backward diffusion and repulsive swarm dynamics: They may pave the road to a number of new backward models for visual computing applications. This is part of our ongoing research as well.

Acknowledgement. Our research activities have been supported financially by the *Deutsche Forschungsgemeinschaft (DFG)* through a *Gottfried Wilhelm Leibniz Prize* for Joachim Weickert. This is gratefully acknowledged.

References

1. Bergerhoff, L., Weickert, J.: Modelling image processing with discrete first-order swarms. In: Pillay, N., Engelbrecht, P.A., Abraham, A., du Plessis, C.M., Snášel, V., Muda, K.A. (eds.) Advances in Nature and Biologically Inspired Computing, vol. 419, pp. 261–270. Springer, Cham (2016)
2. Carrillo, J.A., Fornasier, M., Toscani, G., Vecil, F.: Particle, kinetic, and hydrodynamic models of swarming. In: Naldi, G., Pareschi, L., Toscani, G. (eds.) Mathematical Modeling of Collective Behavior in Socio-Economic and Life Sciences, pp. 297–336. Birkhäuser, Boston (2010)
3. Gilboa, G., Sochen, N.A., Zeevi, Y.Y.: Forward-and-backward diffusion processes for adaptive image enhancement and denoising. IEEE Transactions on Image Processing 11(7), 689–703 (2002)
4. Osher, S., Rudin, L.: Shocks and other nonlinear filtering applied to image processing. In: Tescher, A.G. (ed.) Applications of Digital Image Processing XIV, Proceedings of SPIE, vol. 1567, pp. 414–431. SPIE Press, Bellingham (1991)
5. Perona, P., Malik, J.: Scale space and edge detection using anisotropic diffusion. IEEE Transactions on Pattern Analysis and Machine Intelligence 12, 629–639 (1990)
6. Sapiro, G., Caselles, V.: Histogram modification via differential equations. Journal of Differential Equations 135, 238–268 (1997)
7. Sochen, N.A., Zeevi, Y.Y.: Resolution enhancement of colored images by inverse diffusion processes. In: Proc. 1998 IEEE International Conference on Acoustics, Speech and Signal Processing. pp. 2853–2856. Seattle, WA (May 1998)
8. Welk, M., Weickert, J.: An efficient and stable two-pixel scheme for 2D forward-and-backward diffusion. In: Lauze, F., Dong, Y., Dahl, A. (eds.) Scale Space and Variational Methods in Computer Vision, Lecture Notes in Computer Science, vol. 10302, pp. 94–106. Springer, Cham (2017)